THE ASTROPHYSICAL JOURNAL, 267:465–482, 1983 April 15

A SURVEY OF GALAXY REDSHIFTS. V. THE TWO-POINT POSITION AND VELOCITY CORRELATIONS

MARC DAVIS
Departments of Astronomy and Physics, University of California

AND

P. J. E. PEEBLES
Joseph Henry Laboratories, Princeton University
Received 1982 August 5; accepted 1982 October 12

ABSTRACT

We describe the results of a study of the two-point correlations in the 14.5 m_B CfA redshift survey. We use the distance information provided by the redshifts to estimate the two-point spatial correlation function $\xi(r)$ in a way that is designed to be unbiased by peculiar velocities. The results agree well with what has been found from the deeper angular distributions. In the fiducial model $\xi(r)=(r_0/r)^\gamma$ with $\gamma=1.77$ we find $r_0=5.4\pm0.3\ h^{-1}$ Mpc ($H_0=100\ h$ km s^{-1} Mpc^{-1}). At $r\gtrsim 10\ h^{-1}$ Mpc, $\xi(r)$ seems to steepen and may in fact be negative at $20\lesssim hr \lesssim 40$ Mpc. In existing n-body simulations $\xi(r)$ is poorly modeled by a power law, with more power on small scales and less power on large scales than the data. This confirms the visual impressions that the n-body clusters are too compact and the clusters too homogeneously distributed relative to the data.

The rms line of sight peculiar velocity difference $\sigma(r_p)$ of correlated galaxy pairs seen projected at separation r_p is clearly detected at $hr<5$ Mpc. The results fit quite well to a power law,

$$\sigma(r_p)=340\pm40(hr_p/1\text{ Mpc})^{(0.13\pm0.04)}\text{ km s}^{-1},$$

at 10 kpc $\lesssim hr_p \lesssim 1$ Mpc. The slow variation of σ with r_p would not be expected on scales $r_p<300$ kpc unless the matter is considerably less concentrated than the light of bright galaxies. The mass could be in dark halos extending to this scale. Alternatively the mass could be clustered like the galaxies if matter loosely associated with the fainter galaxies deleted in our analysis carries the bulk of the mass density, so that M/L is a decreasing function of luminosity. We argue that the available evidence tends to favor the latter picture. We derive the cosmological density parameter $\Omega=0.2\ e^{\pm0.4}$ for the component of matter clustered with the galaxy distribution on scales $\leqslant 1\ h^{-1}$ Mpc.

Subject headings: cosmology — galaxies: clusters of — galaxies: redshifts

I. INTRODUCTION

During the past several years there has been considerable work on large-scale redshift surveys in selected regions of the sky. The Harvard-Smithsonian Center for Astrophysics (CfA) survey is the largest presently available sample and is complete to 14.5 m_B in the regions ($\delta>0, b>40°$) and ($\delta\geqslant-2.5°, b<-30°$). Previous papers in this series have discussed data analysis procedures (Tonry and Davis 1979), the overall large-scale distribution and comparisons to existing n-body simulations (Davis *et al.* 1982, hereinafter DHLT), and the luminosity function, the mean density of galaxies, and the peculiar gravity of the Local Supercluster (Davis *et al.* 1980; Davis and Huchra 1982, hereinafter DH). Techniques of group assignment and virial analysis have been discussed by Press and Davis (1982) and by Huchra and Geller (1982). The catalog of redshift data is given in Huchra *et al.* (1982).

Part of the motivation for the survey was to provide a sample for studies of the general statistics of the galaxy distribution and motions. For this purpose the statistical sample should not be directed toward or away from rich clusters: it ought to contain a representative collection of the varieties of groups and clusters found in the universe. As the CfA sample contains three large clusters at well-sampled depths (Virgo, Coma, and A1367), it may for the first time approach this ideal in a redshift sample. We present here the results of an analysis of the two-point position and velocity correlation functions in the CfA sample.

The CfA sample considerably improves our empirical understanding of several important aspects of the galaxy two-point correlation functions. It is known from angular distributions that the spatial correlation function closely approximates a power law, $\xi(r)=(r_0/r)^\gamma$, at $hr \lesssim 10$ Mpc ($H_0=100\ h$ km s^{-1} Mpc^{-1}). That result is confirmed here by direct inversion of the observed function (§ V; Fig. 3 below), where the bias due to peculiar motion is eliminated by integrating along the line of sight. The parameter r_0 has been only crudely estimated (Groth and Peebles 1977), and the CfA sample yields a considerable improvement (Table 1 below). The shape of $\xi(r)$ at $r \sim 10\ h^{-1}$ Mpc is poorly known and is of considerable interest because this is the transition from strongly nonlinear clustering on smaller scales to linear fluctuations ($\delta\rho/\rho < 1$) on larger scales. A model of the expected behaviour of the position and velocity correlation functions at this transition has been derived from the BBGKY hierarchy equations (Davis and Peebles 1977). The CfA results suggest that $\xi(r)$ falls below the power law $(r_0/r)^\gamma$ at $r \gtrsim 10\ h^{-1}$ Mpc, as expected in this model, but the sample is not yet large enough for an unambiguous test (§ IV; Fig. 3 below).

The pattern of relative motions of neighboring galaxies is important as a measure of the nature of the mass distribution and of the amount of mass. One can estimate relative velocities by isolating physical associations or else by the use of statistics of the sort discussed here. Of course, each method has important limitations and so should be considered a complement of the other. The statistic studied here is the distribution of relative line-of-sight peculiar velocities of close pairs of galaxies. This distribution is clearly seen at projected separations hr_p in the range 0.1–5 Mpc, and for the first time we can be fairly sure that the effect is not due to measuring errors or to bias in the catalog (§ VI). In § VII we use the velocity dispersion results to estimate the cosmological density parameter. As in previous papers of this series, we utilize the 20,000-body numerical simulation of cosmological clustering by Efstathiou and Eastwood (1981) to test our procedures throughout and to contrast to the observations.

The discussion in § VIII relates to the behavior of the velocity dispersion as a function of scale size, extending the range to studies of binary galaxies on small scales. We conclude that either isothermal halo mass distributions extend to a scale of $\sim 300\ h^{-1}$ kpc about luminous galaxies, or that most of the clustered missing mass is associated with fainter galaxies. The evidence, though incomplete, favors the second picture.

II. THE SAMPLE

The CfA sample contains 2400 galaxies, of which 1840 are in the North zone $b^{\mathrm{II}} > 40°$, $\delta > 0$. The galaxy redshifts have been corrected for motion in the Local Group and for a peculiar velocity of 440 km s^{-1} toward the Virgo Cluster using procedures identical to those described in previous papers in this series. For the present purposes this is important only because of its effect on the determination of galaxy absolute magnitudes and the luminosity function (DH).

We eliminate the intrinsically faint galaxies,

$$M_B > -18.5+5\log h. \tag{1}$$

A galaxy with this absolute magnitude appears at the catalog magnitude limit at 40 h^{-1} Mpc distance. Eliminating the fainter galaxies reduces the weight of the Local Supercluster, and the resulting catalog is closer to being volume limited. The remaining galaxies are a fairly homogeneous sample, which is an advantage because the clustering statistics of bright and faint galaxies surely differ at some level. We also eliminate the galaxies at distances greater than 100 h^{-1} Mpc, where space sampling is sparse. This leaves 1230 galaxies in the Northern zone.

Redshift measurement errors have been a serious problem in some earlier statistical studies but appear to be comfortably small here. Approximately 60% of the redshifts for this sample are from the CfA survey and have rms error of 35 km s^{-1}. The remaining 40% are from the literature and have errors estimated at 70 km s^{-1} in the mean, although many are high-quality 21 cm observations and others are low-quality optical observations. Only 55 of the 1840 Northern sample galaxy redshift have reported uncertainties of 100 km s^{-1} or larger.

We need the relative probability $\phi(r)$ that a galaxy is included in the sample. We assume that ϕ is a function only of the galaxy distance r. With the absolute magnitude cutoff (eq. [1]) we can set $\phi=1$ at $r < 40\ h^{-1}$ Mpc. For $40 < hr < 100$ Mpc we use the $\phi(r)$ derived by DH in a way that is unaffected by spatial inhomogeneities. DH find $\phi=0.37$ at $hr=60$ Mpc, $\phi=0.095$ at $hr=80$ Mpc. Our distance limit gives $\phi=0$ at $hr > 100$ Mpc.

Though the depth of the sample is considerably larger than the characteristic length $r_0 \sim 5\ h^{-1}$ Mpc where $\xi=1$ (§ V), one expects to find significant density fluctuations on scales greater than r_0. Indeed, such fluctuations are very evident in the maps of the CfA sample (DHLT) and must be borne in mind in the choice of method of statistical analysis and in the assessment of the results. The method of analysis is discussed next.

III. TWO-POINT CORRELATION FUNCTIONS

a) *Definitions*

The precision measures of galaxy positions and motions are the angular position and the redshift of each galaxy. These are conveniently represented as a three-dimensional polar map in a redshift space. We assume that the cosmological redshift is directly proportional to distance and that the galaxy distributions and peculiar motions are a homogeneous and isotropic random process. If peculiar redshifts are negligible, the redshift map is a true space map; peculiar motions distort positions along the line of sight. The two-point correlation function in this redshift map is a function of two variables, the separations parallel and perpendicular to the line of sight:

$$\pi = v_1 - v_2, r_p = [(v_1 + v_2)/H_0] \tan(\theta_{12}/2), \quad (2)$$

with v_1 and v_2 the velocities and θ_{12} the angular separation on the sky. The probability of finding a galaxy in the volume element δV at separation r_p, π from a galaxy is

$$\delta P = n[1 + \xi(r_p, \pi)] \delta V \phi(r), \quad (3)$$

where n is the mean number density and $\xi(r_p, \pi)$ is the two-point correlation function in this redshift space.

When the separation is large, peculiar motions are expected to be unimportant. Here it is useful to ignore the anisotropy in redshift space and measure the two-point correlation as a function of the redshift separation

$$s = (v_1^2 + v_2^2 - 2v_1v_2 \cos\theta_{12})^{1/2}/H_0. \quad (4)$$

The correlation function in s is defined by the usual equation for the probability of finding a neighbor at distance s in any direction,

$$\delta P = n[1 + \xi(s)] \phi \delta V. \quad (5)$$

The statistic $\xi(s)$ is useful because it is simple and can be estimated even when the signal is small [when, for example, the noise is too large to estimate $\xi(r_p, \pi)$]. When $H_0 s$ is large compared to peculiar velocities, $\xi(s)$ approximates the true space correlation function $\xi(r)$. The statistic $\xi(r_p, \pi)$ is a convolution of $\xi(r)$ with the peculiar velocity difference distribution. A model for this convolution is discussed in § VI. Davis, Geller, and Huchra (1978) introduced $\xi(s)$. The statistic $\xi(r_p, \pi)$ was used by Peebles (1976) as a formalized version of the statistical approach introduced by Geller and Peebles (1973). For further discussion of $\xi(r_p, \pi)$ see Peebles (1980*a*, § 76).

b) Methods of Estimation

The role of the apparent-magnitude limit must be carefully considered in the correlation function estimates. Also, there are appreciable density fluctuations on scales comparable to the depth of the CfA sample (DH) which cannot be ignored. We have used two weighting schemes in the estimates of the correlation function. The first counts each pair with equal weight. The second weights each pair ij by $\phi_i^{-1} \phi_j^{-1}$, so each part of space is weighted in proportion to the number of pairs that would be present in a totally volume-limited sample. The most distant pairs carry the most weight in the second scheme, and so we cut off the sample at $r = 80\ h^{-1}$ Mpc, where $\phi(r) \sim 0.1$. The first weighting scheme gives considerably more weight to the foreground clustering. The second scheme is close to the minimum variance weighting for determination of $\xi(r)$. (This follows from an analysis similar to that described in DH.) This is because the second weighting attempts to treat each volume element of the sample on an equal basis. The price paid is an increase in the background white noise level of the power spectrum due to the unequal weighting of pairs. Since $\xi(r)$ is the Fourier transform of the power spectrum, and the small scale is most sensitive to the high-frequency end of the power spectrum, the second weighting scheme yields very noisy measures of $\xi(r)$ on small scales. Another way of saying this is that the small-scale end of $\xi(r)$ is determined by relatively few pairs, so that unequal weighting of the pairs causes very substantial fluctuations. On larger scales, there are many pairs per bin and the increased statistical noise of the discrete counts is more than counterbalanced by the increased effective number of independent spatial groupings averaged together.

Given a suitable weighting scheme, one can count the total pairs in an interval $(\Delta r_p, \Delta\pi)$ or Δs and compare them to what would be expected in the absence of clustering. If the sample were much larger than the clustering length the number density of galaxies expected to be counted at a given distance r would be $n\phi(r)$. Unfortunately, as shown in Figures 5 and 6 of DH, the actual distribution [call it $nc(r)$] departs quite substantially from this curve. In counting pairs, we use the fact that equations (3) and (5) instruct us to count neighbors from the position of each galaxy, not from random locations in the sample. This is a distinction of no significance if the catalog has $c(r) \approx \phi(r)$, but it should not be ignored in the samples currently available where density fluctuations on the scale of the sample depth are appreciable.

Specifically, we form the sum of all pairs in a given interval Δs or $(\Delta r_p, \Delta\pi)$,

$$DD = \sum_i \sum_j w_i w_j n_i n_j, \quad (6)$$

where the n_i, n_j are δ-functions giving the position of each particle, the sum over i sums over all particles in the sample, and the sum over j includes only particles in the proper interval Δs or $(\Delta r_p, \Delta\pi)$ from particle i. The weights w_i, w_j are unity in scheme 1 of equally weighted pairs, and are $w_i = 1/\phi_i$ in scheme 2, where we seek optimal weighting.

To compute the expected background counts, we have generated randomly distributed data sets within the solid angle and depth of the survey and have given the points a luminosity distribution that matches $\phi(r)$ as determined by DH. These samples contain typically 2000 points and are spatially homogeneous, satisfying $\langle V/V_M \rangle = 0.5$, and giving agreement in all methods of determining the mean background density n (see DH for details of three alternative methods for determination of n).

Given this random data set, we compute the cross-count sum

$$DR = \sum_i \sum_j w_i w_j n_i m_j , \tag{7}$$

where w_i, w_j, and n_i are as before but now m_j represents the location of points in the random catalog. The resulting correlation function, $\xi(s)$, is given by

$$1 + \xi(s) = \frac{n_R}{n} \frac{DD(s)}{DR(s)} , \tag{8}$$

where n_R/n is the ratio of the mean density in the random catalog to that of the real data set, and n has been determined using the minimum variance technique described in DH. The advantage of this procedure is that edge effects are automatically accounted for. Edge effects are substantial and otherwise difficult to model for scales $r > 10$ Mpc. For $\xi(s)$ we use $w_i = 1/\phi_i$. At $hs < 2$ Mpc, DR has been smoothed to reduce the shot noise.

To determine $\xi(r_p, \pi)$, which provides better information on small scales, we set $w_i = 1$ and determine the background by a slight variation of equation (7),

$$DR(r_p, \pi) = \sum_i n_i n \phi(r_i \pm \pi/H_0) 2\pi r_p \Delta r_p \Delta\pi f(r_i, \pi, r_p) . \tag{9}$$

Here we sum over each galaxy n_i and compute the total number of neighbors in the interval $\Delta\pi, \Delta r_p$ expected if the sample were homogeneous. The fraction of background objects expected to lie within our observing window is f. It is a different function of r_p and π for each galaxy n_i, and its computation requires more time than all the rest of the calculation. The resulting estimate of $\xi(r_p, \pi)$ is then

$$1 + \xi(r_p, \pi) = \frac{DD(r_p, \pi)}{DR(r_p, \pi)} . \tag{10}$$

In all the estimates, only pairs with $\theta_{12} < 50°$ have been included in the computations of DD and DR.

IV. RESULTS FOR $\xi(s)$

Figure 1 shows the estimates of the redshift correlation function $\xi(s)$ (eqs. [4] and [5]) for the North sample. At $1 \lesssim hs \lesssim 10$ Mpc, $\xi(s)$ approximates a power law with index $\gamma \sim 1.8$. At $s \sim 20\ h^{-1}$ Mpc, $\xi(s)$ passes through zero, and at $30 \lesssim hs \lesssim 50$ Mpc it averages -0.05. This result is not required by our prescription for the determination of $\xi(r)$. If we had required (see Peebles 1980a, § 32)

$$n \int d^3 r \xi(r) = -1 , \tag{11}$$

then in the range of 20–60 h^{-1} Mpc, $\xi(s)$ would have to equal -8×10^{-3} in order to balance the clustering on scales less than 20 Mpc. However, one should also recognize that the background density n is determined only to $\sim 10\%$ accuracy in a sample this size, so the estimates of ξ below 0.1 have substantial uncertainty. The uncertainty in n is discussed by DH, and is larger than one might naively expect simply because of the fluctuations induced by the clustering of galaxies.

As a check we have also estimated $\xi(s)$ from the 273 galaxies in the South sample $b^{\mathrm{II}} < -40°$, $\delta > -2.^{\circ}5$. As there may be some systematic differences between the Zwicky magnitudes in the North and South samples, we use here the selection function $\phi(r)$ determined from the South sample. The results are shown in Figure 3 below. The logarithmic derivative of $\xi(r)$ at $s < 10\ h^{-1}$ Mpc is systematically more negative in the South sample. We suspect this is only a fluctuation due to the small size of the sample. It is an important check that the North and South samples yield comparable values for $\xi(s)$ at $3 \lesssim hs \lesssim 10$ Mpc, and that in both samples $\xi(s)$ passes through zero at $s \sim 20\ h^{-1}$ Mpc. This agrees with the indication of a break from the power law $\xi(r) \propto r^{-\gamma}$ at $r \sim 10\ h^{-1}$ Mpc found in the angular correlation studies (Groth and Peebles 1977). We see no evidence of the tail $\xi(s) \sim 0.7$ at $30 \lesssim hs \lesssim 50$ Mpc claimed by Kirshner, Oemler, and Schechter (1979).

V. RESULTS FOR THE SPATIAL CORRELATION FUNCTION ON SMALL SCALES

At small s, peculiar velocities may cause $\xi(s)$ to differ from the space correlation function $\xi(r)$. To avoid this effect we use the integral of $\xi(r_p, \pi)$ over the redshift difference π to obtain the projected function $w(r_p)$ and then either solve $w(r_p)$ for $\xi(r)$ or else fit $w(r_p)$ to a power law model for $\xi(r)$.

The projected function is defined as

$$w(r_p) = \frac{1}{H_0} \int_{-v_L}^{v_L} d\pi \xi(r_p, \pi) . \tag{12}$$

We use $v_L = 2500$ km s^{-1}. If this is large enough to include almost all correlated pairs and peculiar velocities, then the relation to the space correlation function is

$$\begin{aligned} w(r_p) &= 2\int_0^\infty dy \xi\left[\left(r_p^2 + y^2\right)^{1/2}\right] \\ &= 2\int_{r_p}^\infty r\,dr\,\xi(r)\left(r^2 - r_p^2\right)^{-1/2} . \end{aligned} \tag{13}$$

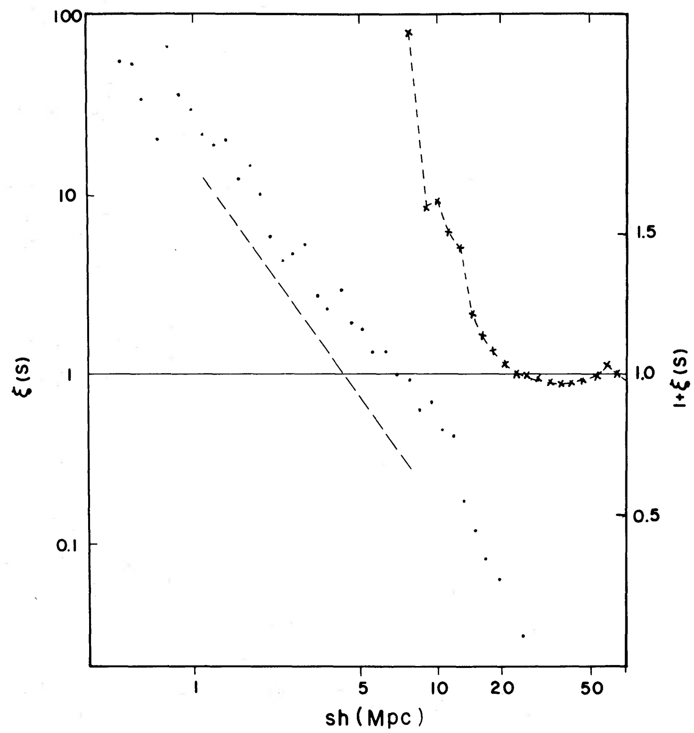

FIG. 1.—Redshift correlation function $\xi(s)$. Dots, $\xi(s)$ on the logarithmic scale on the left; crosses, $1+\xi(s)$ on the linear scale on the right. The dashed line is a power law $s^{-1.8}$.

The inverse is the Abel integral

$$\xi(r) = -\frac{1}{\pi}\int_r^\infty dr_p w'(r_p)\left(r_p^2 - r^2\right)^{-1/2}. \quad (14)$$

Given $w(r_p)$, it is straightforward to numerically evaluate equation (14) for $\xi(r)$, a procedure valid only for $r \ll v_L/H_0$, but certainly the preferred procedure for $r < 10$ Mpc. This inversion is much simpler than the inversion of Limber's equation required to derive $\xi(r)$ from $w(\theta)$ (Fall and Tremaine 1977).

Figure 2 shows $w(r_p)$ for the North sample. The thin line in Figure 3 shows the Abel solution $\xi(r)$. To eliminate the major gradient of the correlation function, we have plotted the product $r^2\xi(r)$. Before the Abel integral is inverted, $w(r_p)$ is smoothed, and the oscillations in $r^2\xi(r)$ at small scale are an artifact of this process. This curve is terminated at 7 Mpc where the procedure is becoming uncertain and affected by the choice of v_L. Also shown are the redshift correlation functions $\xi(s)$ for the northern and southern samples. At $5 \lesssim hr \lesssim 10$ Mpc, where it is reasonable to compare $\xi(r)$ and $\xi(s)$, the results from the northern sample agree well.

The dotted curve in Figure 3 is $r^2\xi(r)$ determined from $w(r_p)$ for the n-body simulation of Efstathiou and Eastwood (1981). The function closely matches that of Efstathiou and Eastwood who derived $\xi(r)$ using the three dimensional position of each particle. This is a welcome check that the $\xi(r)$ derived from the data is a useful measure of the true spatial correlation function,

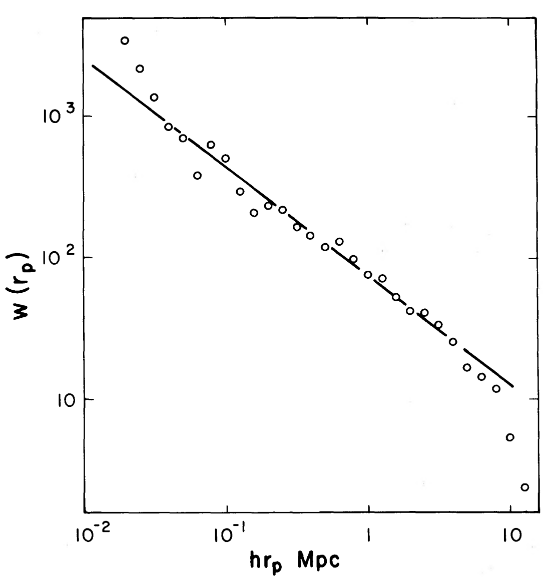

FIG. 2.—Projected correlation function $w(r_p)$ (eq. [12]). The solid line is the power law model (eq. [19]).

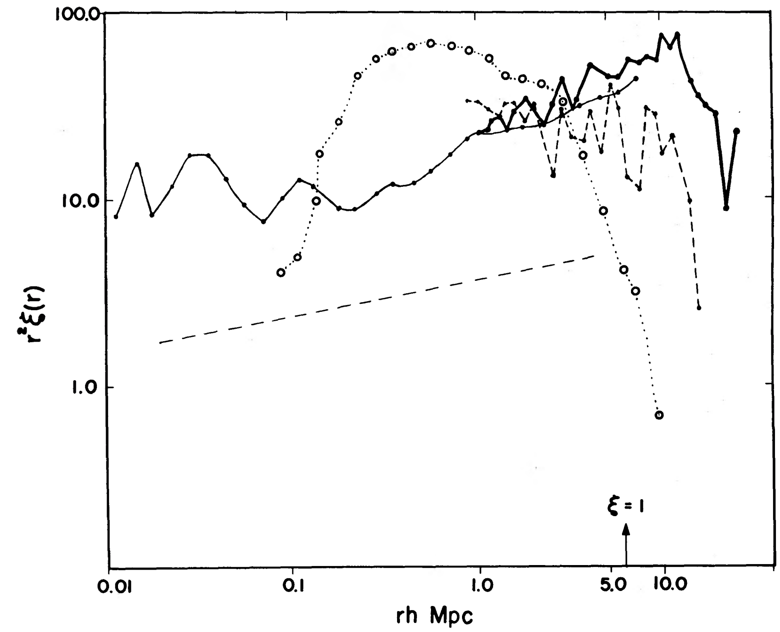

FIG. 3.—The spatial correlation function $r^2\xi(r)$ (eq. [14]) is the light line. The heavy line is $s^2\xi(s)$ from the northern sample, and the ragged dashed line is $s^2\xi(s)$ from the southern sample. A power law $\xi \propto r^{-1.8}$ is indicated by the straight dashed line, while $r^2\xi(r)$ from the n-body simulation is shown as the dotted line connecting open circles.

not unduly biased by redshift distortions or our inversion procedure.

Figure 3 shows that the galaxy spatial correlation function for the Northern sample is quite well approximated by a power law,

$$\xi(r) = (r_0/r)^\gamma, \tag{15}$$

at $r < 10\ h^{-1}$ Mpc. At $H_0 r_p \ll v_L$ equation (13) yields for the power law model

$$w(r_p) = A r_p^{1-\gamma},$$
$$A = r_0^\gamma \Gamma(1/2)\Gamma[(\gamma-1)/2]/\Gamma(\gamma/2). \tag{16}$$

The parameter γ is best derived from Figure 2. A least squares fit to $w(r_p)$ at $r_p < 2\ h^{-1}$ Mpc gives

$$\gamma = 1.74 \pm 0.04. \tag{17}$$

Equation (17) agrees well with the result from the angular correlation studies (Groth and Peebles 1977),

$$\gamma = 1.77 \pm 0.04, \tag{18}$$

where the error comes from a choice by eye of the maximum and minimum slopes and so the stated error is perhaps two standard deviations.

Table 1 shows the results of fits by eye to the range of reasonably acceptable values of r_0 for two choices for γ and using $w(r_p)$ and the Abel solution for $\xi(r)$ at r_p or $r < 2\ h^{-1}$ Mpc. The results from the two methods agree well. Our fiducial estimate is

$$r_0 = 5.4 \pm 0.3\ h^{-1}\ \text{Mpc}, \gamma = 1.77. \tag{19}$$

This is shown as the solid curve in Figure 2.

An analysis along roughly similar lines yielded $r_0 = 4.23 \pm 0.26\ h^{-1}$ Mpc for the redshift sample of Kirshner, Oemler, and Schechter (1978) (Peebles 1979). As this sample was chosen to avoid rich clusters, the discrepancy with equation (19) is not unexpected. Groth and Peebles (1977) found $r_0 = 4.7\ h^{-1}$ Mpc from the angular data. Because this depends on a quite uncertain estimate of the luminosity function, the agreement with equation (19) is as good as one could have hoped.

Integrals useful in the theory of clustering dynamics are

$$J_2(r) = \int_0^r \xi(r) r\, dr, \qquad J_3(r) = \int_0^r \xi(r) r^2\, dr. \tag{20}$$

TABLE 1

CLUSTERING LENGTH

	hr_0[a]	
γ	$w(r_p)$	Abel
1.75 ...	5.5 ± 0.25	5.7 ± 0.3
1.80 ...	5.2 ± 0.25	5.2 ± 0.3

[a]Unit = Mpc.

TABLE 2

CORRELATION INTEGRALS

hR[a]	J_2[b]	J_3[c]
2......	67	32
5......	93	124
10......	112	277
15......	136	544
20......	142	698
25......	145	780
30......	142	684
40......	122	−162
50......	110	−540

[a]Unit = Mpc.
[b]Unit = $h^2\,\mathrm{Mpc}^2$.
[c]Unit = $h^3\,\mathrm{Mpc}^3$.

Table 2 shows estimates of these integrals based on the Abel solution for $\xi(r)$ for $hr < 10$ Mpc and on $\xi(s)$ for $hr > 10$ Mpc. They agree well with estimates from the Lick sample (Clutton-Brock and Peebles 1981),

$$J_2 = 164 e^{\pm 0.15} h^{-2}\ \mathrm{Mpc}^2, \qquad J_3 = 596 e^{\pm 0.21} h^{-3}\ \mathrm{Mpc}^3,$$
$$hr \sim 30\ \mathrm{Mpc}. \qquad (21)$$

As J_3 approximates the second central moment of the counts of objects in a sphere of radius r, we do not expect J_3 to be negative. The estimates at $hr > 30$ Mpc therefore are not to be trusted. However, they do demonstrate that J_3 determined from galaxy clustering is highly uncertain at $hr > 30$ Mpc and cannot reliably be used to calculate expected anisotropies in the microwave background radiation due to the Sachs-Wolfe effect (Peebles 1981*a*).

VI. THE DISTRIBUTION OF RELATIVE VELOCITIES

a) *Results for* $\xi(r_p, \pi)$

A contour map of $\xi(r_p, \pi)$ is shown in Figure 4. The departures of the contours from mirror symmetry about the $\pi = 0$ axis are caused by differences in the background corrections for $(v_i + |\pi|)$ and $(v_i - |\pi|)$ in equation (9). The dashed semicircles show expected contours of $\xi(r_p, \pi)$ if there were pure Hubble flow. The elongations in the π direction demonstrate quite convincingly that the redshift maps are distorted from true spatial distributions by an amount well in excess of what is expected from redshift measurement errors. This map is essentially unchanged if we delete the galaxies within 6° of the Virgo core, and within 3 h^{-1} Mpc of A1367 and Coma and with velocity differences of less than 1500 km s^{-1} from the cluster means.

Figures 5*a*–5*g* show straight averages of the $\xi(r_p, \pi)$ estimates over intervals of r_p spaced by successive factors of 2. We turn next to a numerical analysis of these results.

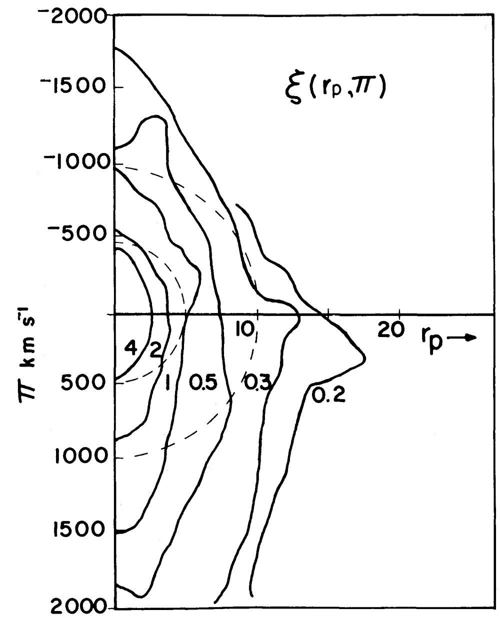

FIG. 4.—The two-point correlation as a function of separations r_p and π perpendicular and parallel to the line of sight. The lines are contours of fixed $\xi(r_p, \pi)$. The dashed semicircles show the expected shape of the contours if peculiar velocities were negligible.

b) *Model for the Relative Velocity Distribution*

The statistic $\xi(r_p, \pi)$ is a convolution of the space correlation function $\xi(r)$ with the distribution f of the relative line-of-sight peculiar velocity. As the second moment of f is found to vary only slowly with r, we use a model in which f is independent of r and of direction (relative to the line joining galaxies). Then

$$1 + \xi(r_p, \pi) = H_0 \int_{-\infty}^{\infty} dy \left\{ 1 + \xi\left[\left(r_p^2 + y^2\right)^{1/2}\right]\right\} f(V),$$
$$V = \pi - H_0 y \left\{1 - h\left[\left(r_p^2 + y^2\right)^{1/2}\right]\right\}. \qquad (22)$$

The term $H_0 y\, h(r)$ represents the mean streaming velocity relative to the Hubble flow: if the clustering is statistically stable on the scale r, then $h(r) = 1$; if the clusters expand with the general expansion, $h = 0$. Following the similarity solution (Davis and Peebles 1977) we expect $h(r)$ is roughly of the form

$$h(r) = F\left[1 + (r/r_0)^2\right]^{-1}, \qquad (23)$$

with $F = 1$. The clusters in the n-body simulations of Efstathiou and Eastwood are slowly collapsing and would be consistent with equation (23) if F were roughly 1.5. We test the sensitivity of the velocity dispersion estimates to the streaming correction $h(r)$ by adjusting the parameter F.

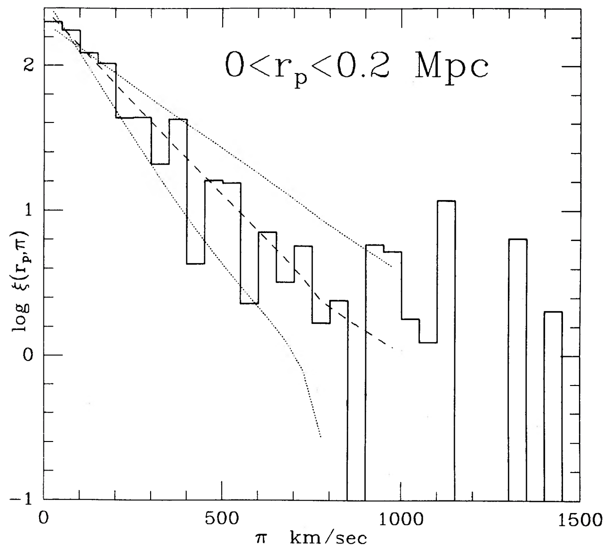

FIG. 5*a*

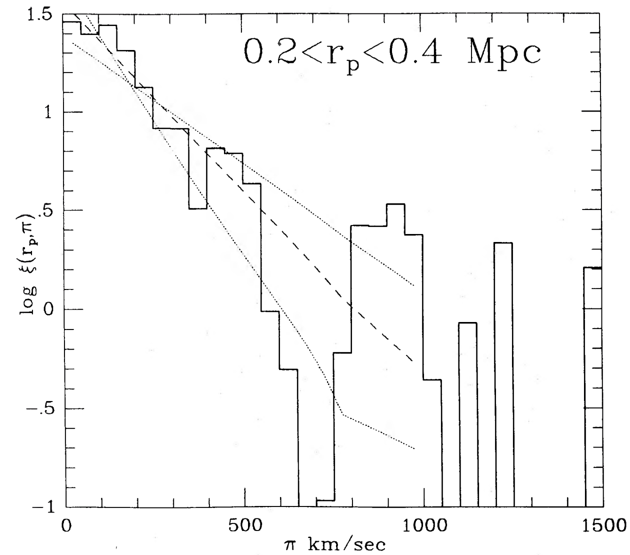

FIG. 5*b*

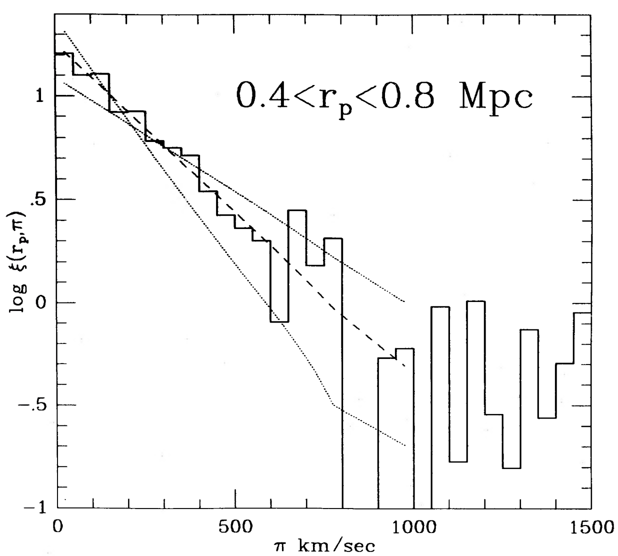

FIG. 5*c*

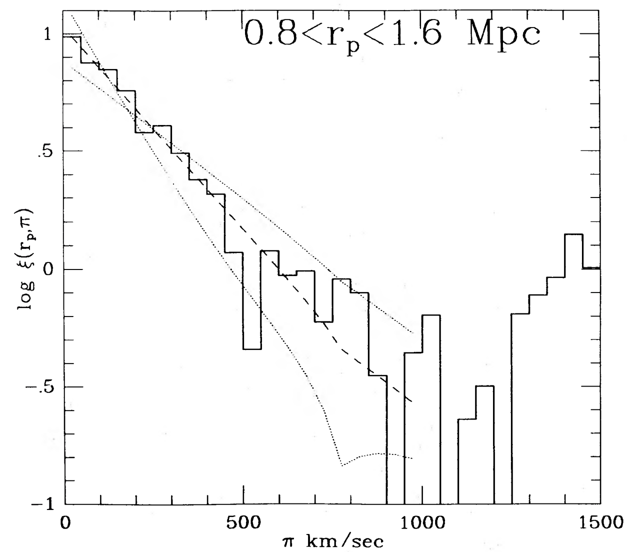

FIG. 5*d*

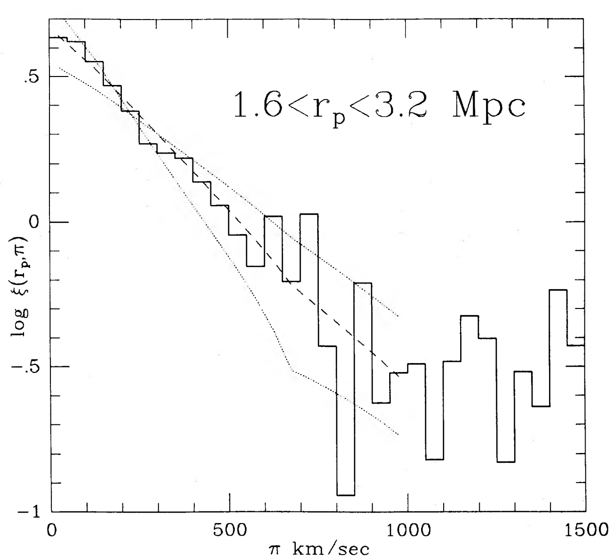

FIG. 5*e*

FIG. 5.—(*a*) The correlation function $\xi(r_p, \pi)$ for $\sigma < r_p < 0.2$. The dashed curve is the fit to the model equations (22)–(24) with $F = 1$ and σ given in Table 3. The dotted curves correspond to the best fit with σ constrained to be 2/3 or 3/2 of its best fit value. (b) Same as Fig. 5*a*, with $0.2 < r_p < 0.4\ h^{-1}$ Mpc. (*c*) Same as Fig. 5*a* with $0.4 < r_p < 0.8\ h^{-1}$ Mpc. (*d*) Same as Fig. 5*a* with $0.8 < r_p < 1.6\ h^{-1}$ Mpc. (*e*) Same as Fig. 5*a* with $1.6 < r_p < 3.2\ h^{-1}$ Mpc. (*f*) Same as Fig. 5*a* with $3.2 < r_p < 6.4\ h^{-1}$ Mpc. (*g*) Same as Fig. 5*a* with $6.4 < r_p < 12.8\ h^{-1}$ Mpc. The dashed line is a model with $\sigma = 450$ km s^{-1}.

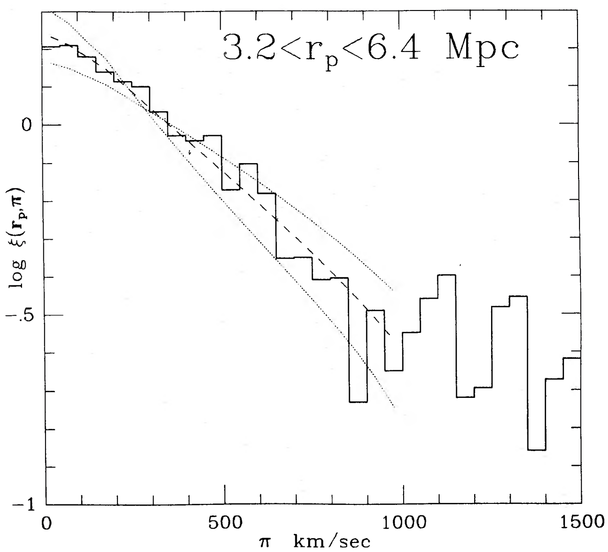

FIG. 5f

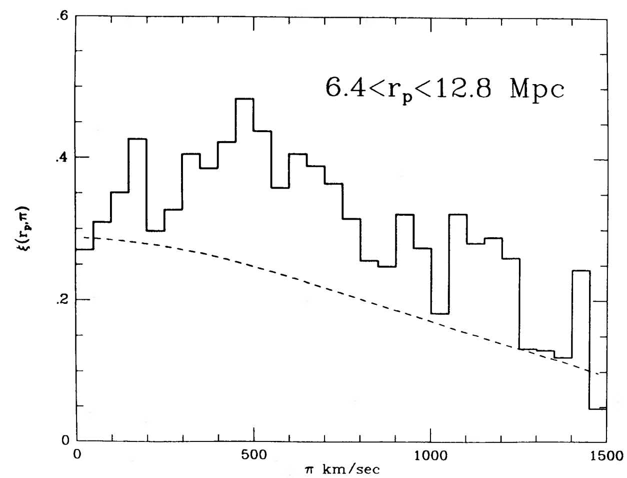

FIG. 5g

In agreement with previous analyses (Peebles 1976) we find better fits to the data if we use an exponential distribution for $f(V)$, rather than a Gaussian or power law model. The curves in Figures 5a–5g show the model for $\xi(r_p, \pi)$ based on the power law model for $\xi(r)$ (eq. [15]) with $\gamma = 1.8$ and $F = 1$ in equation (23); and the exponential model

$$f(V) \propto \exp\left(-2^{1/2}|V|/\sigma\right), \tag{24}$$

and three choices for the rms dispersion. The model with the best fitting value of σ (see next section) is plotted as the dashed curve, and the dotted curves are fits with σ constrained to 2/3 or 3/2 of its best value. The quality of the fits is seen to be excellent with σ well constrained, except in Figure 5g, and a slight trend of σ with r_p is apparent. The estimates of ξ for $|\pi| > 1000$ km s^{-1} are seriously influenced by background corrections, and so little weight can be given to them.

c) *Estimates of the Relative Velocity Dispersion* $\sigma(r)$

We could estimate the dispersion σ from the integral of $\pi^2\xi(r_p, \pi)$, but the integral depends sensitively on ξ at $|\pi| \gtrsim 1000$ km s^{-1} where $\xi(r_p, \pi)$ is poorly known. As the exponential model so closely matches the observed shape of $\xi(r_p, \pi)$, we instead adjust σ and a normalization constant in equation (24) to yield the least squares residuals of the model to $\xi(r_p, \pi)$, considering separately each of the r_p intervals in Figures 5. The normalization constant is necessary to accommodate the small fluctuations of ξ from a pure power law behavior. The results are given in Figure 6 and Table 3 along with representative formal errors for σ with $F = 0.1$, 1, and 1.5 for data in the range $|\pi| < 1000$ km s^{-1}. We do not have the sensitivity to simultaneously fit for F and σ. Tests with $F = 1$ indicate that σ is quite insensitive to the weighting scheme of the fits (either equal weighting or Poisson noise weighting) or to incrementing the velocity limit to $|\pi| < 1500$ km s^{-1}. Again this is indicative of good fits to the model. The fits to the bin $6.4 < r_p < 12.8\ h^{-1}$ Mpc are not listed, as the model is a poor match to the data for any σ. Also listed are results when galaxies in the

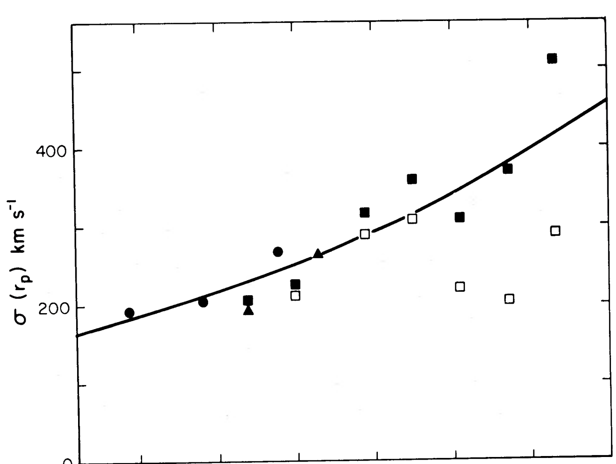

FIG. 6.—The velocity dispersion as a function of projected separation. The filled squares are based on the model fit to $\xi(r_p, \pi)$ with $F = 1$ (eq. [23]); the open squares, on the model with $F = 0.1$. The triangles are second moments of $\xi(r_p, \pi)$. The circles are derived from the Turner sample. The curve is eq. (32).

TABLE 3

DISPERSION FITS

hr_p (Mpc)	DATA: $\|\pi\| < 1000$ km s^{-1} $F=1$	$F=1.5$	$F=0.1$	Delete 3 Clusters $F=1$	SIMULATION $\|\pi\| < 1500$ km s^{-1} $F=1.5$
0–0.2	226 ± 15	231	211	229	602 ± 70
0.2–0.4	317 ± 33	325	290	313	681 ± 60
0.4–0.8	358 ± 22	375	308	337	808 ± 71
0.8–1.6	308 ± 16	337	220	268	844 ± 45
1.6–3.2	369 ± 22	418	204	345	580 ± 40
3.2–6.4	510 ± 30	637	289	739	446 ± 82

cores of the Virgo, Coma, and A1367 clusters are deleted from the sample as described above. Again the effect is minor, demonstrating that σ is a measure of the typical pair dispersion, and is not heavily biased by the infrequent rich cluster.

When the interval $hr_p < 200$ kpc is divided into two parts, we get $\sigma = 206$ km s^{-1} at $hr_p < 100$, but at $100 < hr_p < 200$ we get a value of σ that we suspect is unrealistically large as a result of the noise in the ξ estimates. The latter value is not shown in Figure 6. At small r_p we can more directly estimate σ as the second π moment of ξ because the Hubble flow is small. On truncating ξ at $|\pi| = 750$ km s^{-1} we find the second moments

$$\sigma = 194 \text{ km s}^{-1}, \qquad hr_p < 100 \text{ kpc};$$

$$= 265 \text{ km s}^{-1}, \qquad 100 < hr_p < 200 \text{ kpc}. \qquad (25)$$

These are plotted as the triangles in Figure 6. They fit well onto the trend of σ observed at larger r_p.

Results for the Efstathiou and Eastwood simulation are also indicated in Table 3 but are less satisfactory because of the poor match of $\xi(r)$ to a power law model. The fits for the first two bins are good, but for the second two bins with high σ, the fits are only fair. The behavior of $\sigma(r_p)$ for the simulation is nonetheless consistent with the results given by Efstathiou and Eastwood who measured $\sigma(r)$ directly, with full knowledge of all six degrees of freedom for each point. This again is a welcome check on the validity of our procedure. Note that $\sigma(r_p)$ for the simulation is considerably larger than for the real data, as is apparent upon comparison of the redshift space maps of the two samples (DHLT). Recall that the points in the n-body simulation have been modified to have an rms one-dimensional velocity of 350 km s^{-1}, so that the one-dimensional rms pair difference velocity should be on the order of 500 km s^{-1}. More on this will be discussed below.

On small scales the σ estimates are quite independent of the model (eqs. [22]–[24]), but on larger scales the choice of the model, particularly the choice of F, substantially influences the results. A small value of F implies that galaxies on all scales are expanding with the Hubble flow, so that on large scales the widths of the histograms of Figure 5 are dominated by this Hubble flow. Setting $F=0$ is unreasonable because it says the observed clusters are not bound. By our prescription of equation (23), with $F=1$, galaxies with separations of 5 Mpc are expanding at only *half* the Hubble rate; the Hubble flow is cancelled by counterstreaming on small scales, and the counterstreaming drops rapidly beyond $r = 5\ h^{-1}$ Mpc. This is intuitively as expected and suggests $0.8 < F < 1.5$ for a variety of reasonable models of the clustering, a result consistent with both the present n-body simulations and the BBGKY hierarchy solutions, as discussed above. With F in this range the trend of σ with r_p is not very sensitive to the precise value of F.

d) Estimates of $\sigma(r_p)$ from the Turner Pairs

We can extend the range of estimates of σ as a function of r_p by using the new redshift data for Turner binaries. Turner (1976) chose these galaxies from a deeper sample, $m \leqslant 15$, so there are more close pairs than in the CfA sample. New accurate redshifts based on the methods of the CfA survey are reported by White *et al.* (1982, hereafter WHLD).

Though Turner chose pairs isolated on the sky, they may be expected to approximate a fair sample of all pairs because the typical number of bright galaxies near a close pair is small. The mean number of neighbors of a pair at separation r is given by the three-point correlation function ζ,

$$N = n\xi(r)^{-1}\int d^3z\,\zeta(r,z,|\boldsymbol{r}-\boldsymbol{z}|). \qquad (26)$$

This equation applies at $r \ll r_0$ ($\xi \gg 1$). An accurate model for ζ is (Peebles and Groth 1975)

$$\zeta = Q\{\xi(r)\xi(z) + \xi(|\boldsymbol{r}-\boldsymbol{z}|)[\xi(r)+\xi(z)]\}. \qquad (27)$$

With equation (15) for ξ we find that the ensemble average number of neighbors in a sphere of radius αr

centered on a pair at separation r is

$$N \approx 8\pi Q n r_0^{\gamma}(\alpha r)^{3-\gamma}/(3-\gamma). \tag{28}$$

We are interested in bright galaxies, with mean space density $n \sim 0.01\ h^3$ Mpc^{-3}. With $Q \sim 0.7$ (eq. [46] below) we get

$$N \sim 2.8\ (\alpha h r)^{1.23}, \tag{29}$$

with r in Mpc. With hr equal to the median projected separation $\sim 25\ h^{-1}$ kpc in the Turner sample and $\alpha = 5$, $N \sim 0.2$. That is, most close pairs are well isolated in space. The Turner pairs were selected by a similar criterion for the projected distribution: no neighbors brighter than $m = 15$ appear in a circle of radius 5θ where θ is the angular separation of the pair. This rejects a much larger fraction of pairs than is given by equation (29) because many neighbors only appear close in projection. However, if, as we will assume below, the relative velocity of a galaxy pair at separation r is statistically determined by the mass within distances on the order of r, then we would expect that the relative velocities in the Turner sample approximates a fair sample of all bright pairs.

Figure 7 shows that this is so. The solid histogram is the distribution of relative velocities for all 131 Turner pairs with $\pi < 1000$ km s^{-1}. The dashed histogram is ξ at $hr_p < 200$ kpc normalized to the same area at $\pi < 1000$ km s^{-1}. The two are very similar. For example, we expect from the normalized ξ to find 5.0 pairs at 600–1000 km s^{-1} and observe five Turner pairs; at 400–600 km s^{-1}, 6.1 are expected and nine observed; at 300–400 km s^{-1}, 10.1 are expected and seven observed.

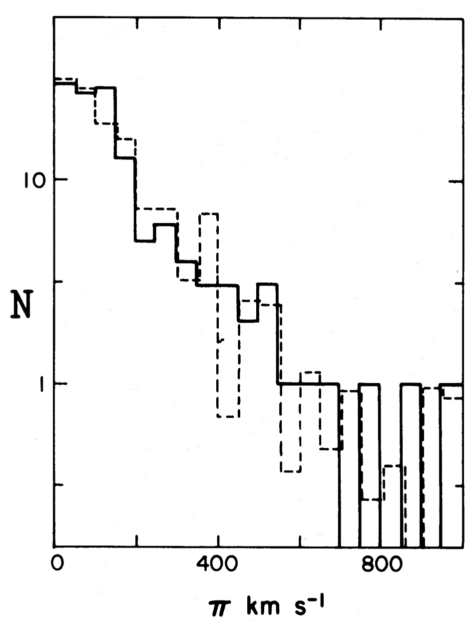

FIG. 7.—The distribution of relative velocities. The solid histogram is the distribution for the full Turner sample. The dashed histogram is $\xi(r_p, \pi)$ for $hr_p < 200$ kpc and scaled to the same area at $\pi < 1000$ km s^{-1}.

To estimate $\sigma(r_p)$ from the Turner pairs we must eliminate accidentals without unduly truncating the intrinsic distribution. Our method is based on the fact that the distribution in π looks like the exponential model (eq. [24]), which also proved successful for $\xi(r_p, \pi)$. When this distribution is truncated at $n\sigma$, the second moment is

$$\langle \pi^2 \rangle = \sigma^2 \frac{1-(n^2+2^{1/2}n+1)\exp(-2^{1/2}n)}{1-\exp(-2^{1/2}n)}. \tag{30}$$

We compute $\langle \pi^2 \rangle$ for the distribution truncated at π_0 and then solve this equation for σ. The results for three choices of π_0 are shown in Table 4. If there were serious contamination by accidentals, σ would increase with increasing π_0 and increasing r_p; if our model for the intrinsic distribution of π had too broad a tail, σ would tend to decrease with increasing π_0. No substantial trends with π_0 or r_p are seen, so we adopt a straight average of the three σ estimates for each r_p bin. They are plotted as the circles in Figure 6.

e) Discussion of the Results

We fit the estimates of $\sigma(r_p)$ to a power law model,

$$\sigma(r_p) = \sigma_0 (hr)^{\delta}. \tag{31}$$

We exclude the data at $hr > 1.6$ Mpc because they are very sensitive to the clustering expansion model, and we use the two second moments of ξ instead of the model fit at $hr_p < 200$ kpc. A least squares fit of log σ to log r_p using the model fits to $\xi(r_p, \pi)$ with $F = 1$, the second

TABLE 4
VELOCITY DISPERSION IN THE TURNER SAMPLE

Separation[a]	N	π_0	$\langle \pi^2 \rangle^{1/2}$	σ[b]
$5 < hr_p < 15$	35	750	217	238
	33	500	167	198
	30	350	119	143
$15 < hr_p < 45$	48	750	185	193
	47	500	167	198
	45	350	146	223
$45 < hr_p < 135$ ...	30	750	245	286
	28	500	202	292
	25	350	146	223

[a]Unit = kpc.
[b]Unit = km s^{-1}.

moments of ξ, and the Turner sample results, with equal weight per point, gives $\sigma_0 = 344$ km s^{-1} (r in Mpc) and $\delta = 0.133 \pm 0.04$. If we change from $F = 1$ to $F = 0.1$, we get $\sigma_0 = 280$, $\delta = 0.07$. Here the last point (0.8–1.6 Mpc) is well below the curve. If we eliminate this point, we get $\sigma_0 = 333$, $\delta = 0.127$ with the $F = 0.1$ model. As was discussed above, $F \sim 1$ is more realistic than $F = 0.1$ so the $F = 1$ results deserve more weight. Our fiducial best fit is then

$$\sigma = (340 \pm 40)(hr_{\rm Mpc})^{0.13 \pm 0.04} \text{ km s}^{-1},$$
$$10 \text{ kpc} \lesssim hr_p \lesssim 1 \text{ Mpc}. \quad (32)$$

Figure 6 shows that this curve fits the data quite well to $hr_p \sim 800$ kpc and, if the $F = 1$ model is to be trusted, to ~ 6 Mpc. The stated uncertainty in σ_0 is our estimate of how far up or down it might be reasonable to move the curve.

Using methods similar to what has been described here, Peebles (1976) found $\sigma \sim 200$–600 km s^{-1} in the de Vaucouleurs Reference Catalog; Davis, Geller, and Huchra (1978) found $\sigma = 300 \pm 30$ km s^{-1} from the $B \leqslant 13.0$ redshift sample (roughly, the Shapley-Ames sample); Peebles (1979) found $\sigma \sim 450$ km s^{-1} from the Kirshner-Oemler-Schechter (1978) sample, and Peebles (1981*b*) found $\sigma = 450 \pm 100$ km s^{-1} from the Rood (1982) compilation. As the CfA sample is considerably better suited to this purpose, equation (32) supersedes these earlier results. In an analysis similar to that described here of the deep AAT redshift survey which contains some 300 galaxies, Bean *et al.* (1982) found values of σ in the range 200–250 km s^{-1}, and their data are consistent with no trend of σ with r. The increased noise of their smaller sample decreases their ability to identify such a trend.

Rivolo and Yahil (1981) found in the revised Shapley-Ames catalog (Sandage and Tammann 1981) $\sigma = 100 \pm 15$ km s^{-1} at $r_p \lesssim 0.35$ h^{-1} Mpc. They obtained quite similar results for isolated pairs and for the sample of all close pairs. This is significantly lower than our result. A possible reason is that Rivolo and Yahil found the background correction in the estimation of a statistic similar to $\xi(r_p, \pi)$ by fitting the distribution in π to a sum of two Gaussians, each with adjustable variance and amplitude, one to represent correlated pairs, the other to represent the background. The background correction thus determined need not be a good estimate of the ensemble average background. As the revised Shapley-Ames catalog does not very closely approximate a fair sample of the universe, that need not be a consideration, but it does make it difficult to judge whether the Rivolo-Yahil procedure unduly truncates the distribution of π for physical pairs. Another point of disagreement is that we find $f(V)$ in the CfA sample to be well approximated by an exponential model, while Rivolo and Yahil find a good fit with a Gaussian model. It seems likely that the Rivolo-Yahil procedure with exponentials rather than Gaussians would yield larger values of σ because the broader exponential tail can take up more of the neighbors at large $|\pi|$ that are assigned to the background in the Gaussian model.

VII. THE DENSITY PARAMETER

We present two estimates of the cosmological density parameter, one based on the Irvine-Layzer cosmic energy equation (Fall 1975; Davis and Peebles 1977; Davis, Geller, and Huchra 1978), the other on dynamic stability of the clustering at $r \lesssim 1$ h^{-1} Mpc (Geller and Peebles 1973; Peebles 1976).

a) *Energy Equation*

The cosmic energy equation relates the single-galaxy one-dimensional velocity dispersion $\bar{v}_p$ to the potential energy stored in fluctuations assuming $\xi(r)$ measures the underlying mass distribution; the differential equation can be approximated as an algebraic equation (Peebles 1980*a*, eq. [74.6]),

$$\bar{v}_p^{\,2} \approx \tfrac{2}{7} H_0^{\,2} J_2(\infty)\,\Omega. \quad (33)$$

If $\xi(r)$ is negligibly small at $r \geqslant 20$ h^{-1} Mpc, then Table 2 says $J_2 h^2 \sim 150$ Mpc^2, which yields

$$\Omega \approx (\bar{v}_p/660)^2. \quad (34)$$

The chief difficulty with this test is the determination of $\bar{v}_p$ from the measurements of $\sigma(r)$. Whereas $\sigma(r)$ is a pair-weighted dispersion that gives high weight to the rich groups, $\bar{v}_p$ equally weights each galaxy. Furthermore, $\bar{v}_p$ includes large-scale coherent velocity fields that are unobservable from $\sigma(r)$ on small scales. If $\xi(r)$ has a long-range positive tail, it increases J_2 and J_3, the latter increasing correlated motions and $\bar{v}_p/\sigma$ (Clutton-Brock and Peebles 1981). In linear perturbation theory these two effects just cancel, so a positive tail at $r \geqslant 20$ h^{-1} Mpc might not seriously bias our estimate of Ω.

In the self-similar BBGKY solution (Davis and Peebles 1977) $\bar{v}_p$ and $\sigma(r)$ are roughly equal to each other at a scale of 1 h^{-1} Mpc. On the other hand, in the n-body simulation of Efstathiou and Eastwood (1981) $\sigma(r)$ at $r \sim 1$ h^{-1} Mpc is approximately twice $\bar{v}_p$, both in the $\Omega = 1$ and $\Omega = 0.1$ simulations, and $\sigma(r)$ decreases with scale size, as expected for the shape of $\xi(r)$ in the simulation. As long as the effective power law of $\xi(r)$ is steeper than $\gamma = 2$, $\sigma(r)$ must decrease with r if the behavior is self-similar.

The simulation data are consistent with σ roughly constant at 600 km s^{-1} for $r_p < 1$ Mpc, although σ decreases on larger scales. If $\bar{v}_p$ is half this value, then from equation (34) we expect $\Omega = 0.09$ for the simulation, in complete agreement with the procedure used by DHLT to display this simulation, in which $\bar{v}_p$ was constructed to be 350 km s^{-1}.

In the real data, if we assume $\sigma(1\ \text{Mpc}) = \bar{v}_p$ as expected from the similarity solution, we find from equation (34) the estimate

$$\Omega = 0.27. \tag{35}$$

This determination obviously is limited by the uncertainty in the relation of $\sigma(r)$ to $\bar{v}_p$.

b) *Statistical Stability Condition*

Our second estimate of Ω is based on the assumption that the mass clustering on scales $\lesssim 1\ h^{-1}$ Mpc is statistically stable, not expanding with the general expansion and not collapsing. The balance condition at $r < r_0$ is (Peebles 1976; Davis and Peebles 1977; Peebles 1980*a*, § 75)

$$\begin{aligned} &\frac{\partial[\xi(r)\langle v^\alpha v^\beta\rangle]}{\partial r^\beta} \\ &= -g^\alpha(r)\xi(r) = -2G\rho\int d^3z\,\zeta_\rho z^\alpha/z^3 \\ &\approx -2Gm(r)\xi(r)r^\alpha/r^3 - 2Gm(r)n\int d^3z\,\zeta z^\alpha/z^3. \end{aligned} \tag{36}$$

The Cartesian components of the relative velocity of a pair of galaxies at separation r^α are v^α, and $\langle v^\alpha v^\beta\rangle$ is an average over a fair sample of pairs at separation r^α. The mean gravitational acceleration of one of the pair as seen by an observer at rest on the other is g^α. This can be written as an integral over a mass correlation function ζ_ρ, where the ensemble average value of the mass in the volume element d^3z at position z^α relative to one of a pair of galaxies at separation r^α is

$$dM = \rho\xi(r)^{-1}\zeta_\rho(r, z, |\boldsymbol{r} - \boldsymbol{z}|)\,d^3z, \tag{37}$$

where ρ is the mean mass density. Now we can imagine apportioning this mass among the bright galaxies, so that $m(r)$ is the mean mass per bright galaxy within distance r; this mass could be in a smooth halo or it could be in the halos of faint companions. Then as indicated in the last of equations (36), g^α can be written as the sum of the direct gravitational interaction of the pair and the mean effect of all the neighbors of the pair. If the mass is concentrated in and around bright galaxies, then at $hr \gtrsim 300$ kpc g^α is dominated by neighbors of the pair so we can set g^α equal to the second term in the last of equation (36) with $\rho = mn$ (§ VIII*c* and eq. [29]). The same is true even at small r if mass is arranged in a scale-invariant clustering hierarchy. We adopt this approximation in the following analysis, and in § VIII*c* we return to a discussion of the direct interaction term in the last of equations (36).

We shall assume galaxies are good tracers of the way mass is clustered so ζ is given by the galaxy three-point function in equation (27). The main justification for this is that it implies $\sigma \propto r_p^{0.115}$ (eq. [45] below), quite close to the observed behavior (eq. [32]). The first term in equation (27) for ζ makes no contribution to g, the integral over the second term is easily evaluated, and the third term yields a complicated integral that makes a somewhat larger contribution because of a peculiar feature of the model. At small z, $\xi(z)$ is large, and as there is a nonzero gradient of $\xi(|\boldsymbol{r} - \boldsymbol{z}|)$ at $z \to 0$, these two factors with $\cos\theta$ yield an appreciable contribution to the peculiar acceleration of the galaxy at $z = 0$ toward the galaxy at $\boldsymbol{z} = \boldsymbol{r}$ by the mass concentrated around $z = 0$. As this seems unreasonable, we replace the third term with the second. This gives

$$g(r)r = 6Q(Hr)^2\xi(r)\Omega/(3-\gamma). \tag{38}$$

As the estimates of $\sigma(r_p)$ have substantially improved, it is worthwhile to treat the left-hand side of the stability equation (36) in more detail than has been done heretofore. The velocity moment can be written as (Davis and Peebles 1977)

$$\langle v^\alpha v^\beta\rangle = A(r)\left(\delta_{\alpha\beta} + br^\alpha r^\beta/r^2\right). \tag{39}$$

Following White (1981) we assume b is constant and A varies as $r^{2\delta}$ (eq. [31]). Then with $\xi \propto r^{-\gamma}$ equation (36) becomes

$$rg(r) = A(r)[(\gamma - 2\delta)(1+b) - 2b], \tag{40}$$

where $g = |g^\alpha|$. The anisotropy parameter b is related to White's parameter e by the equation

$$e = (1+b)/(3+b). \tag{41}$$

For isotropic orbits, $b = 0$; for purely radial orbits, $b \gg 1$; and for purely circular orbits, $b = -1$.

If the orbits are radial, the gravitational acceleration can be quite small (e.g., Hartwick and Sargent 1978; Peebles 1980*b*; Tremaine and Ostriker 1982; WHLD). The reason is easy to see: in a stationary state with zero gravitational acceleration, radial orbits yield $\xi \propto r^{-2}$, close to what is observed. However, this is a contrived situation (and impossible to maintain in a clustering hierarchy) so we suspect there is little reason to doubt the traditional assumption $b \sim 0$ in the present application.

If Hubble flow can be neglected, the velocity dispersion observed at projected separation r_p is

$$\sigma^2 = \frac{\int dy\,\xi(r)A(r)(1+by^2/r^2)}{\int dy\,\xi(r)}, \tag{42}$$

where $r^2 = r_p^2 + y^2$. As White (1981) showed, if ξ and A vary as powers of r, the integral can be reduced to tabulated functions. For the present case we obtain

$$\sigma^2(r) = KA(r),$$

$$K = \frac{\gamma - 2\delta + b}{\gamma - 2\delta} \frac{\Gamma[(\gamma - 2\delta - 1)/2]\Gamma(\gamma/2)}{\Gamma[(\gamma - 2\delta)/2]\Gamma[(\gamma - 1)/2]}. \quad (43)$$

This is equivalent to White's equation (16). With $\gamma = 1.77$ and $b = 0$, $K = 1.456$ if $\delta = 0.15$; $K = 1.306$ if $\delta = 0.115$, the value used below; and $K = 1$ if $\delta = 0$. This analysis does not apply to the model used to estimate σ at large r_p, but it ought to give the general trend of the relation between σ and A and so we adopt the correction factor K throughout.

Equations (38), (40), and (43) give

$$\sigma^2(r) = 6CQ(H_0 r)^2 \xi(r)\Omega,$$

$$C = K[(\gamma - 2\delta)(1 + b) - 2b]^{-1}(3 - \gamma)^{-1}. \quad (44)$$

Since $\xi \propto r^{-\gamma}$, this model says

$$\delta = 1 - \gamma/2 = 0.115, \quad (45)$$

which agrees with the fit in equation (32).

Estimates of ζ in the Rood (1982) sample give $Q = 0.68 \pm 0.05$ (Peebles 1981*b*). Pending analysis of ζ in the CfA sample we adopt

$$Q = 0.7 \pm 0.2. \quad (46)$$

With $\delta = 0.115$, $\sigma_0 = 340 \pm 40$ km s^{-1} (eq. [32]), and $b = 0$, we get

$$\Omega = 0.20 e^{\pm 0.4}. \quad (47)$$

This agrees with the estimate from the energy equation (eq. [35]). The stated error in equation (47) is about equally from σ and Q. The accuracy of the latter certainly can be improved by a three-point analysis of the CfA sample. We hope to be able to report on the results of that study in due course.

The luminosity density in the Zwicky B magnitude system in the CfA sample is (DH)

$$j = 1.1 \times 10^8 \, hL_0 \, \text{Mpc}^{-3}. \quad (48)$$

With equation (47) we get

$$M/L \sim 600 \, hM_0/L_0. \quad (49)$$

VIII. DISCUSSION

a) The Spatial Two-Point Correlation Function

The estimates of the galaxy spatial correlation function $\xi(r)$ at $r \lesssim 10 \, h^{-1}$ Mpc are well approximated by a power law, the index γ agreeing with what was found from the statistics of angular distributions within the error $\sim 3\%$, the value for r_0 differing from the previous estimate by only 13%. This is an important check of two assumptions, that the CfA sample is a fair sample of the universe and that the angular distributions fairly reflect the spatial clustering of galaxies. If the CfA sample were not representative, we would not expect to find that $\xi(r)$ agrees with the results from the deeper samples of galaxy angular distributions. Almost all estimates of $\xi(r)$ from angular distributions have assumed that patchy obscuration may be neglected. Uson and Seldner (1982) have carefully examined the hypothesis that an appreciable part of the apparent clustering in the Lick and deeper samples is due to patchy absorption. They conclude that this would require a significant increase in γ and decrease in r_0, which would spoil the agreement with the CfA results.

The redshift information in the CfA sample greatly reduces the chance of systematic errors arising from the luminosity function or variable obscuration. Thus, we believe equation (19) is the best available estimate of r_0.

The power law behavior of $\xi(r)$ extending over three decades of length scale remains a most remarkable feature of galaxy correlations, a feature poorly modeled in existing simulations. There are hints of departures from a pure power law for $r < 0.1 \, h^{-1}$ Mpc, where $\xi(r)$ may be slightly steeper than the mean, and for $5 < r < 10 \, h^{-1}$ Mpc, where $\xi(r)$ is slightly shallower. However, even if the ensemble of galaxy clustering were describable as a pure power law, small departures would be expected in any relatively small sample such as the one under consideration here. The comparison of $\xi(r)$ in Figure 3 to that of the n-body simulation is illuminating because it clearly demonstrates the differences between these two samples which are so apparent by visual inspection. Note how $r^2\xi(r)$ is larger in the simulation than in the data on small scales, $r < 3.5 \, h^{-1}$ Mpc, but is smaller on larger scales. This confirms the impression that the simulation clusters are tighter and more centrally concentrated, with the virial motion in the clusters easier to detect in the redshift maps. On the other hand, the individual clumps are more homogeneously distributed than in the real data.

As the characteristic length r_0 is only $\sim 5\%$ of the CfA depth, one might wonder why there are such prominent density fluctuations in the CfA maps (DHLT). One can understand the significance of r_0 as follows. Suppose $\xi(r) = (r_0/r)^\gamma$ to very large r, and suppose a sphere with diameter $4r_0$ is placed at random. The rms fluctuation in the number of galaxies found in the sphere is $\delta N/N = 0.73$ (Peebles 1980*a*, eq. [59.3]). That is, we expect that the density averaged over the scale $\sim 4r_0 \sim 20 \, h^{-1}$ Mpc fluctuates by a factor of about 2, as is observed.

If the sphere diameter is increased to the CfA depth $\sim 100 \, h^{-1}$ Mpc, we get $\delta N/N \sim 0.2$ for a pure power law $\xi(r)$, and $\delta N/N \sim 0.1$ for a power law truncated at $r = 20\ h^{-1}$ Mpc. Thus, the mean galaxy number density derived from the CfA sample may have an intrinsic uncertainty of about 15%. As the estimate of $1+\xi$ is the ratio of observed to expected numbers of neighbors, one might conclude that the ξ estimates from the CfA sample are uncertain to at least ± 0.15. That would be true if we normalized the counts of neighbors in the sample by the ensemble average number density. However, because the number density also is estimated from the sample, the statistical noise in the ξ estimates is reduced by a cancellation of effects: if the sample happens to contain an unusually large number of galaxies, the observed number of neighbors will tend to be larger than the ensemble average and the expected number used in the denominator also will be too big, which tends to cancel the fluctuation. This effect can be analyzed, but as it depends on the galaxy four-point correlation function which is poorly known, the results are not very interesting. We only note therefore, that the expected fluctuations around the mean depend on the number of independent clumps present. Thus in our sample ξ falls below zero at $20 \lesssim r \lesssim 40\ h^{-1}$ Mpc, which is a length scale sufficiently large compared to the sample volume for there to be only a few spatially independent groupings. This negative correlation zone mainly reflects the fact that in the CfA northern sample there is an underabundance of galaxies with velocities $3000 < V < 6000$ km s^{-1}. This hole is quite real, but of course the problem is to decide whether the situation is typical, and the only true guide is the degree of reproducibility of results from independent samples. A similar behavior of $\xi(r)$ has been reported by Shanks (1982) in an analysis of the Durham/AAT and Kirshner, Oemler, and Schechter (1978) redshift samples, which suggests that galaxies on average are anticorrelated on scales in excess of 20 h^{-1} Mpc.

The North and South CfA samples and the Lick catalog all indicate that $\xi(r)$ breaks from the power law $r^{-\gamma}$ at $r \sim 10$–$20\ h^{-1}$ Mpc. The first and last of these samples are the best available for the detection of such a feature, and the coincidence of results is suggestive, but as we have noted, we cannot yet exclude the assumption that we are seeing only sampling fluctuations. If the break is real it is an important and highly suggestive effect because it occurs about at the transition between characteristically linear and nonlinear fluctuations. In particular, such a feature appears in the $\Omega = 1$ similarity solution (Davis and Peebles 1977; Davis, Groth, and Peebles 1977).

b) *Peculiar Velocities*

The continuing controversy over the galaxy rms peculiar velocity, whether derived from identification of physical associations or from statistical analyses of the ensemble, is in large part due to the difficulty of eliminating the accidental background and foreground galaxies. It is widely recognized that inclusion of accidentals can inflate the estimate of the velocity dispersion; perhaps it is less widely emphasized that truncation of the high-velocity tail can artificially reduce the dispersion. The analysis used here has the advantage that we can specify a background correction that is known to be unbiased within our general assumptions. Of course, there is still the problem of sampling fluctuations. Within the present data the evidence that fluctuations have not grossly affected the estimates of the dispersion $\sigma(r_p)$ is that $\xi(r_p, \pi)$ is found to be quite a smooth function of π and r_p with a width in π that is well in excess of what would be expected from the width of $\xi(r)$ (Figs. 5).

Since our analysis is based on counts of pairs, it weights dense regions most heavily and so one could wonder whether our σ estimates only reflect the known high velocities in the richer clusters. There are several reasons for thinking that that is not so: (1) The width of $\xi(\sigma_p, \pi)$ is seen to be unchanged when the galaxies from the cores of the three richest clusters are deleted from the sample (Table 3). (2) The Turner sample of close pairs is biased against dense regions, but we have seen that the relative velocity distribution is indistinguishable from that of the CfA sample (Fig. 7). (3) If σ were determined by the rare high-velocity pairs in rich clusters, $\xi(r_p, \pi)$ would have a sharp spike at small π and a very nearly flat tail extending perhaps to 2000 km s^{-1}, which certainly does not match the observed exponential distribution. (4) The density of pairs decreases rather rapidly with increasing separation, as $r^{-1.77}$. As the crossing time at $hr < 1$ Mpc is much less than the Hubble time, it is reasonable to assume that the density is statistically stable in a crossing time. This is possible if relative orbits are very nearly radial or else if the majority of pairs at separation r are gravitationally bound at mean separation on the order of r. As the first possibility seems artificial, we conclude that most close pairs are bound and are not high-velocity objects only accidentally and temporarily seen close together.

Our $\sigma(r_p)$ estimates also depend on the accuracy of the exponential model for $f(V)$ (eq. [24]). As the model fits the data quite well, the one thing we can imagine going wrong here is that $f(V)$ may depart from the exponential model at $V \gtrsim 1000$ km s^{-1}. If f falls below the model, σ is little affected; if f is above the model, it could substantially increase σ.

We have supplemented the CfA data with the larger number of close pairs in the deeper Turner sample. As these pairs were chosen not to have bright neighbors, they tend to be in less dense regions where the velocity dispersion may be expected to be less than the mean. Thus the circles in Figure 6 may be underestimates of σ for a fair sample, but as close pairs in any case tend not to have many bright neighbors close in space, we suspect the error is not large.

Our estimates of the relative velocity dispersion $\sigma(r_p)$ at small r_p can be compared to what is expected from the typical velocity of stars in a galaxy. We will suppose that the mass distribution within a typical galaxy produces a roughly flat rotation curve at $hr \sim 10$ kpc, which is about the minimum of the range of our estimates of σ as a function of r_p. We assume also that when two galaxies are close, the masses add so the mean relative acceleration is $g = 2v_c^2/r$, where v_c is the rms circular velocity in an isolated galaxy. The assumed flat rotation curve means $\delta = 0$, so equations (40) and (43) yield

$$v_c^2 = \frac{\gamma(\gamma + \gamma b - 2b)}{2(\gamma + b)}\sigma^2. \tag{50}$$

For isotropic orbits this says $\sigma = 0.94 v_c$. Our power law fit to $\sigma(r_p)$ (eq. [32]) yields $\sigma = 187$ km s^{-1} at $hr = 10$ kpc, which would imply $v_c = 176 \pm 21$ km s^{-1}. This is slightly lower than the expected rms circular velocity $v_c \sim 200$–230 km s^{-1} for bright galaxies, which might be an indication that σ has been underestimated, or it might reflect an error in the model for g or in the adopted orbit parameters. The discrepancy is reduced if δ is reduced, but that is not an attractive possibility because in isolated spirals the rotation curve is seen to increase slowly with increasing γ, suggesting $\delta > 0$. Perhaps more likely is the point of WHLD that close binary orbits might be expected to tend to be circular. For example, $b = -0.5$ (which corresponds to rms radial velocity $v_r = 0.45v$, compared to $v_r = 0.58v$ for isotropic orbits) yields $v_c = 214 \pm 25$ km s^{-1}, a quite reasonable value. Thus we conclude that within the uncertainty of the orbit parameters our estimate of σ at small r_p is not unreasonable.

It is worth emphasizing finally that the σ estimates are comfortably large compared to the measuring errors.

Though we have reason to believe our estimates of σ at $hr \lesssim 1$ Mpc are reliable measures of the CfA sample, we cannot be sure this is a fair sample of the universe. An indication of the large-scale fluctuations to be expected is provided by the Soneira-Peebles (1978) clustering prescription where the one-dimensional peculiar velocity distribution approximates an exponential and the broad tail of this distribution is the result of the broad distribution of clump richnesses in this model. As the rare richest clumps make a large contribution to the velocity dispersion, we may expect to find appreciable sampling fluctuations even in large samples. For example, in the Soneira-Peebles prescription, half of σ^2 is due to the richest clumps with 12 levels. In a volume equal to the CfA sample region the expected number of these richest clumps is $nV \sim 0.3$. Thus, the true error in equation (32) as a measure of the universal value of σ may very well exceed the internal error we have quoted.

The result $\sigma \sim 340$ km s^{-1} at $r \sim 1\ h^{-1}$ Mpc is surprisingly large by some measures. Particularly striking is the fact that the one-dimensional mean random velocity of very nearby field galaxies is of order 100 km s^{-1} (Sandage and Tammann 1982). However, one should note two aspects of the peculiar velocities. In the exponential model that we have seen fits the data quite well, 25% of the pairs have relative peculiar velocities $|V| < 0.2\sigma$. That is, as the distribution has a fairly broad tail, a significant fraction of the galaxies have quite small velocities. Second, the high-velocity pairs are expected to appear not at random but rather strongly concentrated in the denser spots. Thus, the 30 nearest galaxies do not represent 30 independent samples of the peculiar velocity distribution. It therefore seems not unreasonable that these neighbors should have rms peculiar velocity relative to us on the order of 0.3σ.

c) *The Nature of the Mass Distribution and the Mean Mass Density*

The mass distribution problem centers on the familiar result that the mass in galaxies is much less than what is implied by our estimate $\Omega \sim 0.2$. For example, if the mass of the universe were dominated by bright galaxies, mean number density $n = 0.01\ h^3$ Mpc^{-3}, each galaxy having a halo truncated at $r_h = 50\ h^{-1}$ kpc, which is about as far as flat rotations curves have been measured in isolated spirals, the rms circular velocity at r_h being $v_c \sim 200$ km s^{-1}, which is typical for spirals (e.g., Rubin, Ford, and Thonnard 1980 and references therein), then $\Omega \sim 0.02$. This is a factor ~ 10 below the result from the last section. Thus if the estimate of Ω from the redshift data is to be believed, r_h must be considerably increased or else the mass of the universe must be dominated by mass around the more numerous faint galaxies.

We can examine this point in somewhat more detail by writing the mean relative peculiar acceleration of galaxy pairs at separation r (eq. [36]) as the sum of the contributions from the mass clustered in and around each of the pairs and from the masses associated with neighbors,

$$rg(r) \sim 2Gm(r)/r + 16\pi QGm(r)n\xi(r)r^2/(3-\gamma). \tag{51}$$

As in equation (36), the mean mass per massive galaxy within distance r of a massive galaxy is $m(r)$, and we assume that this mass is statistically independent of the number of neighbors. With $n = 0.01\ h^3$ Mpc^{-3} this equation becomes

$$rg(r) \sim 2Gm(r)r^{-1}\left[1 + 2.8(hr)^{1.23}\right] \sim 1.18\sigma(r)^2. \tag{52}$$

The last equation follows from equations (40), (43), and (45) with $b = 0$. This equations says that if the mass of the universe were in the high surface brightness parts of bright galaxies, then we should have seen $\sigma \propto r^{-1/2}$ at 10 kpc $\lesssim hr \lesssim 300$ kpc, which certainly does not accord with the observations.

Since there seems to be little doubt that σ is nearly constant at 10 kpc $\lesssim hr_p \lesssim 1$ Mpc, the mean mass around a bright galaxy must vary about as $m(r) \propto r$ to $hr \sim 300$ kpc. This mass could be in smooth halos of the sort needed to account for the rotation curves of isolated spirals at $hr \lesssim 50$ kpc (Rubin, Ford, and Thonnard 1980 and references therein), or it could be associated with the faint galaxies that tend to cluster around bright galaxies. There is some evidence for the latter picture.

If only bright galaxies contribute substantially to the mass density, n is low and a coincidence is required so that $m(r)$ becomes constant just as the second term in parenthesis dominates in equation (52). Otherwise $\sigma(r)$ would show substantial deviations from a power law over this region. If, on the other hand, the bulk of the mass is associated with fainter galaxies, then n is effectively larger, $m(r)$ could converge at $r \sim 50$ kpc, and a power law behavior of σ would be expected. Since faint and bright galaxies seem to have very similar clustering properties, the bright galaxies serve as tracers of the mass distribution in this picture, and the result $\delta \sim (2-\gamma)/2$ is understandable.

Further evidence for this picture comes from the binary galaxy study. WHLD examined the field of each Turner pair in an attempt to find those that are "truly" binaries. As Turner already had eliminated pairs with bright neighbors, WHLD mainly tested for faint companions. The culling narrowed the distribution of velocity differences, which suggests the faint galaxies make a substantial contribution to the mass.

There are some indications that galaxy masses are not very strongly correlated with their luminosities. WHLD considered the model $m \propto L^\alpha$, and tentatively proposed $\alpha = 0.25$. From analysis of the IR–Tully Fisher relation for spiral galaxies, Burstein (1982) suggests that surface brightness varies as Δv^n, $n \sim 2.7$, where Δv is the flat rotational velocity. Since $L \propto \Delta v^m$, $m \sim 4$, then if the objects are rotationally supported we have $\alpha = 1/2 + (2 - n/2)/m \approx 0.66$. Similarly, Romanishin *et al.* (1982) conclude that low surface brightness spiral galaxies have higher than normal M/L ratios, i.e., $\alpha < 1$. The faint end of the galaxy luminosity function often is modeled as $N(<M) \propto \mathrm{dex}(\beta M)$. In this power law model with $m \propto L^\alpha$, the mass diverges at the faint end unless $\alpha > 2.5\beta$. Estimates of the slope of the faint end of the luminosity function range from $\beta = 0.25$ (Abell 1962) to $\beta = 0.1$ (Schechter 1976; Felten 1977) to $\beta = 0.04$ (Kirshner, Oemler, and Schechter 1979) and $\beta \approx 0$ for the CfA sample (DH). These numbers put the critical value of α in the range 0–0.6, and certainly admit the possibility that the mass of the universe is dominated by matter associated with faint galaxies, although it certainly is not confined within the optical boundaries of the faint galaxies.

Within our data the strongest evidence that our result $\Omega = 0.2$ may be seriously in error is the discrepancy between our estimate of $\xi(r_p, \pi)$ and the exponential model at large separations, $hr_p \gtrsim 6$ Mpc, where we see high-velocity tails not expected in the model (Figs. 5*f*, *g*). Larger samples of redshifts will be needed to decide whether this is an accidental fluctuation or an indication that we have missed a broad-spaced mass component.

There are other indications that mass is more broadly distributed than galaxies. Press and Davis (1982) studied the masses of groups identified in the same CfA data set used here. They found that the mass per galaxy varies about in proportion to the cluster diameter up to scales of several megaparsecs. For groups with just two bright galaxies that is just the effect discussed above. Our result at $hr_p \lesssim 1$ Mpc would have led us to believe that the mass per galaxy is constant when the groups contain several bright members. The Press-Davis result is most striking for the smaller clusters, while the larger clusters have more scatter. The Press-Davis correlation is an overall fit to the trend of clusters of all sizes, and is mostly determined by the behavior of the data on small scales.

We note also that the Press-Davis estimate of Ω is consistent with our results $\Omega \sim 0.2$. At still larger scales, estimates of the peculiar velocity field around the Virgo cluster suggest values for Ω in the range 0.2–0.7 (DH; Aaronson *et al.* 1982; Davis 1982). Unless the Virgocentric infall is less than 250 km s^{-1}, this is not consistent with our result, suggesting the possibility that we have missed a weakly clustered mass component.

We thank Simon White for helpful discussions. This research was supported in part by the National Science Foundation grants AST80-00876, AST81-18557, and PHY81-18157.

REFERENCES

Aaronson, M., Huchra, J., Mould, J., Schechter, P. L., and Tully, R. B. 1982, *Ap. J.*, **258**, 64.
Abell, G. O. 1962, *Problems of Extragalactic Research*, ed. G. R. McVittie (New York: Macmillan), p. 213.
Bean, A. J., Efstathiou, G., Ellis, R. S., Fong, R., Peterson, B. A., and Shanks, T. 1983, in preparation.
Burstein, D. 1982, *Ap. J.*, **253**, 539.
Clutton-Brock, M., and Peebles, P. J. E. 1981, *A.J.*, **86**, 1115.
Davis, M. 1982, in *Cosmology and Fundamental Physics* (Scripta Varia, No. 48).
Davis, M., Geller, M. J., and Huchra, J. 1978, *Ap. J.*, **221**, 1.
Davis, M., Groth, E. J., and Peebles, P. J. E. 1977, *Ap. J.*, **212**, L107.
Davis, M., and Huchra, J. 1982, *Ap. J.*, **254**, 437 (DH).
Davis, M., and Peebles, P. J. E. 1977, *Ap. J. Suppl.*, **34**, 425.
Davis, M., Tonry, J., Huchra, J., and Latham, D. 1980, *Ap. J.* (*Letters*), **238**, L113.
Davis, M., Huchra, J., Latham, D., and Tonry, J. 1982, *Ap. J.*, **253**, 423 (DHLT).
Efstathiou, G., and Eastwood, J. W. 1981, *M.N.R.A.S.*, **194**, 503.

Fall, S. M. 1975, *M.N.R.A.S.*, **172**, 23p.
Fall, S. M., and Tremaine, S. 1977, *Ap. J.*, **216**, 682.
Felten, J. E. 1977, *A.J.*, **82**, 861.
Geller, M. J., and Peebles, P. J. E. 1973, *Ap. J.*, **184**, 329.
Groth, E. J., and Peebles, P. J. E. 1977, *Ap. J.*, **217**, 385.
Hartwick, F. D. A., and Sargent, W. L. W. 1978, *Ap. J.*, **221**, 512.
Huchra, J., Davis, M., Latham, D., and Tonry, J. 1982, *Ap. J. Suppl.*, in press.
Huchra, J., and Geller, M. J. 1982, in preparation.
Kirshner, R. P., Oemler, A., and Schechter, P. L. 1978, *A.J.*, **83**, 1549.
______. 1979, *A.J.*, **84**, 951.
Press, W. P., and Davis, M. 1982. *Ap. J.*, **259**, 449.
Peebles, P. J. E. 1976, *Ap. Space Sci.*, **45**, 3.
______. 1979, *A.J.*, **84**, 730.
______. 1980*a*, *The Large-Scale Structure of the Universe* (Princeton: Princeton University Press).
______. 1980*b*, in *Cosmologie Physique*, ed. R. Balian, J. Audouze and D. N. Schramm (Amsterdam: North-Holland), p. 216.
______. 1981*a*, *Ap. J.*, **243**, L119.
______. 1981*b*, in *Proceedings of the Tenth Texas Symposium on Relativistic Astrophysics*, ed. R. Ramaty and F. C. Jones (*Ann. NY Acad. Sci.*, **375**, 157).
Peebles, P. J. E., and Groth, E. J. 1975, *Ap. J.*, **196**, 1.
Rivolo, A. R., and Yahil, A. 1981, *Ap. J.*, **251**, 477.
Romanishin, W., Krumm, N., Salpeter, E., Strom, K., and Strom, S. 1982, *Ap. J.*, **263**, 94.
Rood, H. J. 1982. *Ap. J. Suppl.*, **251**, 477.
Rubin, V. C., Ford, W. K., and Thonnard, N. 1980, *Ap. J.*, **238**, 471.
Sandage, A., and Tammann, G. A. 1981, *Revised Shapley-Ames Catalog* (Washington: Carnegie Institution of Washington).
______. 1982, in *Cosmology and Fundamental Physics* (Scripta Varia, No. 48).
Schechter, P. L. 1976, *Ap. J.*, **203**, 294.
Shanks, T. 1982, in *Progress in Cosmology.*, Vol. **99**, ed. A. W. Wolfendale (Dordrecht: Reidel), p. 335.
Soneira, R. M., and Peebles, P. J. E. 1978, *A.J.*, **83**, 845.
Tonry, J., and Davis, M. 1979, *A.J.*, **84**, 1511.
Tremaine, S., and Ostriker, J. P. 1982 *Ap. J.*, **256**, 425.
Turner, E. L. 1976, *Ap. J.*, **208**, 20.
Uson, J., and Seldner, M. 1982, preprint.
White, S. D. M. 1981, *M.N.R.A.S.*, **195**, 1037.
White, S. D. M., Huchra, J., Latham, D., and Davis, M. 1982, *M.N.R.A.S.*, in press (WHLD).

MARC DAVIS: Department of Astronomy, University of California, Berkeley, CA 94720

P. J. E. PEEBLES: Joseph Henry Laboratories, Princeton University, Princeton, NJ 08544